


Fluctuation-induced spin nematic order in magnetic charge ice

Journal Article

Author(s):

Hemmatzade, Amirreza; Essafi, Karim; [Taillefumier, Mathieu](#) ; Müller, Markus; Fennell, Tom; Derlet, Peter Michael

Publication date:

2024-06-01

Permanent link:

<https://doi.org/10.3929/ethz-b-000680772>

Rights / license:

[Creative Commons Attribution 4.0 International](#)

Originally published in:

Physical Review B 109(22), <https://doi.org/10.1103/PhysRevB.109.224423>

Fluctuation-induced spin nematic order in magnetic charge ice

A. Hemmatzade ¹, K. Essafi ², M. Taillefumier ³, M. Müller ², T. Fennell ^{1,*} and P. M. Derlet ^{2,†}

¹Laboratory for Neutron Scattering and Imaging, *Paul Scherrer Institut, CH-5232 Villigen PSI, Switzerland*

²Laboratory for Theoretical and Computational Physics, *Paul Scherrer Institut, CH-5232 Villigen PSI, Switzerland*

³CSC-Swiss National Supercomputing Centre, *ETHZ, Lugano CH-6900, Switzerland*



(Received 11 April 2024; accepted 4 June 2024; published 20 June 2024)

A pyrochlore charge ice consisting of two magnetic cation types gives rise to a Heisenberg magnet with an interesting type of long-range correlated bond disorder. If the antiferromagnetic exchange among cations of the same type dominates over the interspecies exchange, closed antiferromagnetic chains following the fully packed loops of like cations emerge as nonlocal effective low-temperature degrees of freedom. Monte Carlo simulations reveal a fluctuation driven first-order phase transition from an algebraically correlated spin liquid to a long-range ordered spin nematic, which mean-field theory captures with very high accuracy. The global $O(3)$ Heisenberg symmetry is suddenly reduced to a Z_2 Ising symmetry as the Néel vectors of the strongly antiferromagnetically correlated loops align with each other to optimize the entropy of their thermal fluctuations. Interestingly, the nematic transition is found to be sensitive to the size statistics of the cation loops and thus provides a direct thermodynamic probe of otherwise elusive structural properties. In turn this sensitivity offers a structural route to engineering the nematic phase stability.

DOI: [10.1103/PhysRevB.109.224423](https://doi.org/10.1103/PhysRevB.109.224423)

I. INTRODUCTION

The discrete translational symmetry of the crystalline state underlies the utility of many functional materials. Introducing random disorder into crystalline materials can play a crucial role in modifying their static and dynamical properties to obtain new or improved functionality, for example by producing pinning centers in superconductors [1] or tuning transition temperatures in multiferroics [2,3]. Recently it has been suggested that a kind of correlated disorder based on tiling high-symmetry lattices with low symmetry motifs may be a route to novel functionalities via the interplay of the disorder with crystal properties such as lattice dynamics or electronic conduction [4]. Magnetism is another material property that may be controlled by disorder. Usually uncorrelated variations of exchange strength or coordination (via uncorrelated doping of magnetic ions) are expected to produce spin glasses [5]. In the present work, we show that more correlated types of structural disorder may result in distinct equilibrium and out-of-equilibrium properties.

An ice rule is a well known way to produce such correlated disorder. Here, a simple constraint on the local configuration of binary degrees of freedom allows the construction of an extensively degenerate manifold of states, in which the

correlation among local degrees of freedom decays not exponentially, but by a power-law [6]. Ice rules have a long history beginning with water-ice [7,8], in which the H_2O molecule retains its identity, producing a lattice of O atoms in which the positions of the H define a two-in–two-out displacement ice rule. This motivated a class of Hamiltonians referred to as vertex models, which afford analytical solutions in two dimensions [9], such as the F -model [10]. Such rules and models are of contemporary relevance for describing spin configurations in geometrically frustrated magnetic materials, notably spin ice [11] and quantum spin ice [12]. Ice rules and vertex models also underpin the understanding of artificial spin ice [13–16] and pyrochlore thin films [17,18].

The equivalence of spins and charges on the pyrochlore lattice was first noted by Anderson in an investigation of the Vewey transition in magnetite [19], where it was pointed out that cations would obey a charge ice rule which requires that each tetrahedron is occupied by two cations of each type. If the different cations carry magnetic moments one obtains a model of magnetic charge ice, which is directly relevant to pyrochlores of the type $AMM'F_6$ (for example $CsCrNiF_6$, see Ref. [20]). In pyrochlores such as $R_2MM'O_7$ and $AA'M_2F_7$, see respective Refs. [21,22], the charge ice formed among the nonmagnetic spectator ions may introduce more subtly correlated bond disorder among the magnetic atoms. More generally, geometric frustration of charge order causes correlated site distributions of ions and thus of the interactions among their associated degrees of freedom, resulting in specific material properties that reflect the correlated nature of the underlying disordered structure.

Here we study a nearest neighbor classical Heisenberg Hamiltonian whose exchange constants are templated by the correlated disorder of a charge ice. Using the Monte Carlo

*Contact author: tom.fennell@psi.ch

†Contact author: peter.derlet@psi.ch

method we discover a previously unnoticed order-by-disorder driven first-order phase transition to a low-temperature spin nematic phase, in which the aligning magnetic degrees of freedom are nonlocal and entirely defined by the particular realization of correlated charge ice disorder. The transition is quantitatively described by a mean-field calculation in which each spin experiences an emergent rotation symmetry-breaking Ising anisotropy. Thus, while the spin nematic does not break time-reversal symmetry, it reduces the continuous Heisenberg symmetry to a discrete Ising symmetry, causing a drastic and abrupt increase of the relaxation time entailing an effective spin-freezing in long-lived patterns defined by the underlying disorder.

The paper is organized as follows: In Sec. II we outline the employed sample preparation and numerical methods. Section III details the Monte Carlo results showing the presence of a first-order nematic phase transition and the dependence of its properties on the particular charge ice realization, in particular its loop statistics. Section IV rationalizes the numerical results by first analyzing the thermal properties of a single tetrahedron and then presenting a mean-field theory of the full system, which captures the location of the first-order transition surprisingly accurately. Section V concludes with an emphasis on how correlated disorder can result in distinct equilibrium–out-of-equilibrium behavior and be used to tune emergent nonlocal magnetic degrees of freedom.

II. METHODS

A. Charge ice sample creation

In a simple model of magnetic charge ice [24], two types of magnetic cations a and b populate the pyrochlore lattice according to the 2 : 2 charge ice rule, resulting in correlated site disorder characterized by a randomly packed set of single cation-type nearest-neighbor connected loops of even length. The loops are fully packed, meaning that every cation belongs to a loop [23].

To produce a pyrochlore sample satisfying the charge ice constraint on each tetrahedron, the pyrochlore lattice of size L (containing $N = 16L^3$ cations) is constructed and initially populated with a and b sites according to an ordered structure of $[110]$ and $[1\bar{1}0]$ chains of sites of one or the other type of cation, respectively. Under periodic boundary conditions, this may be seen as a regular array of $4L^2$ winding loops of length $4L$. The loop connectivity of this ordered structure is characterized by any two loops sharing either zero or one tetrahedron. This initial structure will be referred to as the ordered charge ice system I, an example of which is displayed in Fig. 1(a). To produce a disordered charge ice, a string of alternating site types, closing on itself, is identified via a worm algorithm and the ion types of the sites on this loop are interchanged, preserving the charge ice rule. This procedure is repeated until variations in loop structure satisfy the known statistical properties of the loops as detailed in Ref. [23]. Such samples with correlated disorder will be referred to as a charge ice system [see Fig. 1(b)]. For clarity, the figure captions refer to these structures as disordered charge ice.

Figure 1(c) shows the loop size distribution derived from multiple $L = 20$ charge ice realizations, in which we

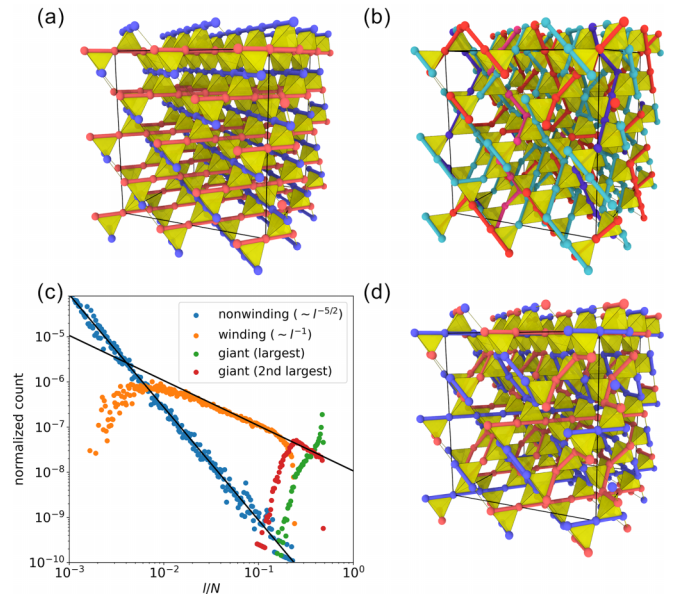


FIG. 1. (a) An ordered charge ice I structure, in which bonds connect nearest neighbor cations of the same type. (b) An example of a disordered charge ice structure realized by eight loops of lengths 42, 30, 16, 14, 8, and $(3 \times) 6$. Here the two largest loops are winding and the remaining are nonwinding. (c) Sample-averaged normalized histogram of loop lengths in which nonwinding and winding are distinguished, as well as the two largest (giant) loops. The power-law exponents are well understood from the perspective of diffusion [23]. The normalized distributions of loop lengths l are plotted as a function of l/N where $N = 16L^3$ with $L = 20$. (d) An ordered charge ice structure II. In panels (a) and (d) cations and bonds are colored according to cation type, whereas in (b) they are colored according to the loop index. In panels (a), (b), and (d) small $L = 2$ samples are used for ease of visualization.

distinguish four classes of loops: those that are nonwinding or winding with respect to the periodic boundaries of the system, and, additionally, the largest and second-largest winding loop. For a given charge ice realization these latter two will be of different chemical type and we refer to them as giant loops. The fraction of sites occupied by the four loop classes tends (with increased sampling and system size) to $f_{nw} = 0.06$ for nonwinding, $f_w = 0.22$ for winding, $f_2 = 0.31$ and $f_1 = 0.41$ for the second and largest (giant) loops respectively, in agreement with Ref. [23].

An alternative ordered charge ice system may be constructed consisting of (001) planes of $[110]$ chains of sites separated by planar regions densely packed with inclined hexagonal loops of length $l = 6$. This structure is referred to as the ordered charge ice system II. It contains L^2 loops of length $4L$ and $2L^3$ of length six [see Fig. 1(d)]. In this structure the system-spanning linear chains (loops) do not share any tetrahedra with each other.

A number of considerations motivates the use of these samples. While the disordered charge ice allows for a realization of algebraically correlated structural disorder resulting in a broad range of loop lengths (up to $\approx L^3$) and nontrivial loop-loop connectivity (shared tetrahedra), the ordered charge ice systems result in just one system spanning loop length

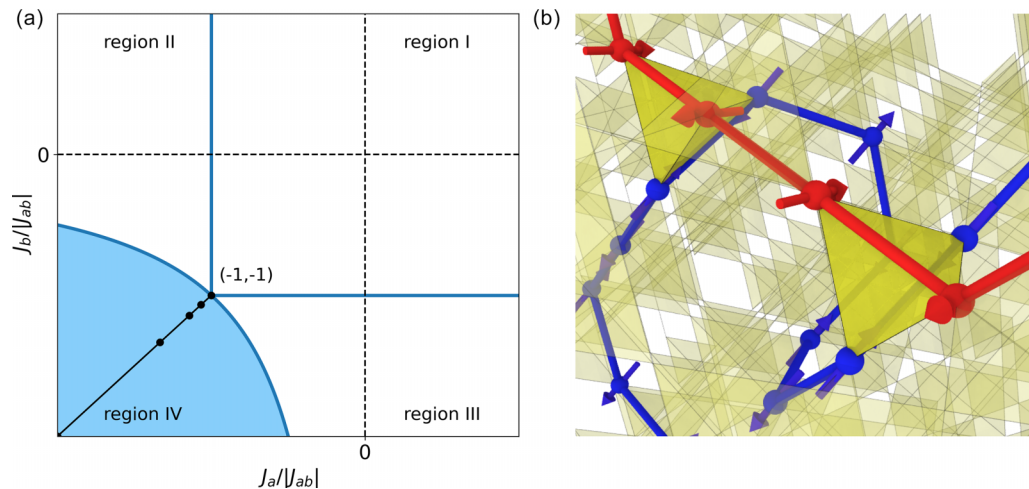


FIG. 2. (a) The ground-state phase diagram [24] is found to be rich in structure with regions I–III hosting long-range ordered phases. The boundary of region IV ($J_{aa}J_{bb} = J_{ab}^2$) contains the classical PHAFM at $(-1, -1)$. Within region IV the ground state is a (less degenerate) classical spin liquid with perfect AFM order on each loop but no correlations between loops. This work focuses on $J_{aa} = J_{bb} = J$ with $J_{aa}J_{bb} = J^2 > J_{ab}^2$ with the simulated system parameters indicated by dots. (b) The charge ice structure of two types of cations, a and b , distributed on the pyrochlore lattice is characterized by an ensemble of closed loops of the same cation species. Two loops of different species (blue and red) may share a number of tetrahedra. In region IV, the ground state is characterized by such loops being AFM ordered but randomly orientated, with respect to each other.

($\approx L$), where each such loop shares at most one tetrahedron with another linear loop in system I, while in system II such loops share no tetrahedra. When templated to a magnetic Hamiltonian (see Sec. II B), these quite diverse loop structures are found to sensitively affect the thermal magnetic properties.

B. Model Hamiltonian: Strong and correlated magnetic exchange disorder via a charge ice

To produce a magnetic charge ice system, we take a charge ice structure and use this to template an exchange network. We describe the magnetic structure by unit-length classical Heisenberg spins on the sites, that are connected by the nearest neighbor exchange constants J_{aa} , J_{bb} , and J_{ab} . The resulting Heisenberg Hamiltonian therefore displays correlated bond disorder that derives from the spatial structure of the cation loops. Banks and Bramwell [24] identified four regions of the ground-state magnetic phase diagram for this model, as shown in Fig. 2(a). In region I, the spins of the same site type are aligned and spins of different type are aligned either parallel or antiparallel according to the sign of J_{ab} . In regions II and III (which are equivalent upon interchange of site type), spins of one type are parallel, with the other type partially frustrated and canted away from the collinear axis of the first type. We focus on region IV, where $J_{aa}J_{bb} > J_{ab}^2$, with J_{aa} and J_{bb} both promoting intraspecies antiferromagnetic (AFM) alignment, so that the zero-temperature ground states have perfect AFM arrangements on each loop [Fig. 2(b)], but are degenerate with respect to the orientation of the AFM alignment axis (the Néel vector) of any loop due to the interloop couplings J_{ab} being perfectly frustrated. In the work of Ref. [24], Monte Carlo simulations at $T/|J| < 0.12$ for region IV ($J_{aa} = J_{bb} = J$ with $J/|J_{ab}| = -1.2$) revealed a pinch-point-like structure factor and a vanishing Edwards-Anderson parameter down

to $T/|J| = 0.012$ (indicating no spin freezing), suggesting an algebraic spin liquid down to arbitrarily low temperatures.

To investigate yet lower temperatures and study the fate of the spin liquid, we have used a single-site Monte Carlo approach. Since a wide range of temperature scales are to be probed, the Monte Carlo heat bath algorithm was found to be most suitable. Here, a Monte Carlo move entails randomly selecting a site and calculating exactly the probability density function for that spin with all other spins fixed. This distribution is then sampled to determine a new configuration for the chosen spin. While there is a computational cost in sampling this distribution, it has the advantage of all moves being accepted and of automatically reducing the scale of variations in spin as the temperature is decreased. For more details see, for example, Ref. [25].

III. NUMERICAL RESULTS

We now numerically investigate how the ground-state properties of region IV manifest themselves at finite temperature. In doing so, we find that large enough loops align themselves below a temperature scale characterized by a first-order phase transition. This temperature scale is found to depend sensitively on both the loop length distribution and the ratio $J/|J_{ab}|$.

A. Low-temperature spin nematic order

Focusing on the fully antiferromagnetic case $J_{aa} = J_{bb} = J < 0$ with $J/|J_{ab}| = -2$ (region IV), our Monte Carlo simulations show that, on cooling ($0.125 \lesssim T/|J| \lesssim 1.5$), the system evolves from the paramagnetic state into a low-temperature state with an energy per site approaching that of the expected ground-state value, a strongly suppressed magnetization, and a well developed plateau in the specific heat

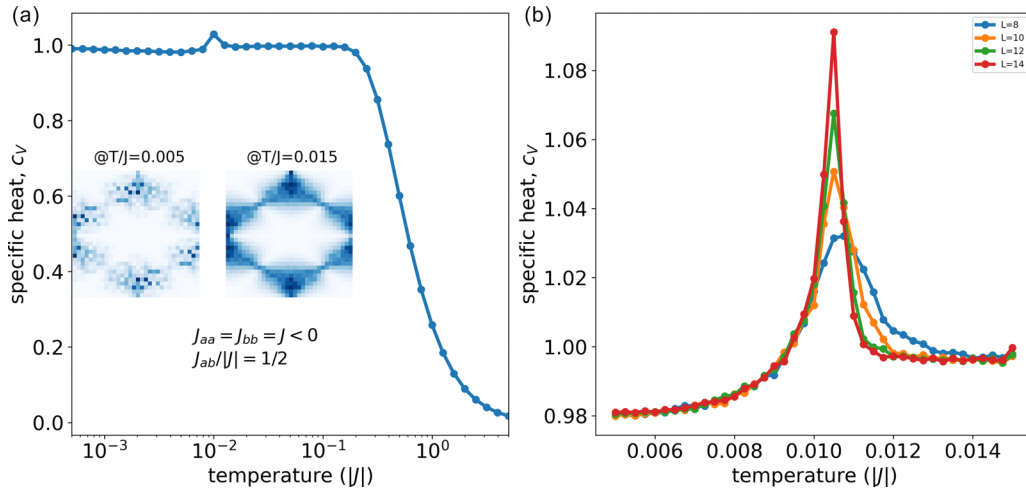


FIG. 3. Specific heat as a function of temperature for a parameter set in region IV, indicating (a) a low-temperature plateau and a peak, which (b) sharpens with increasing system size, signifying a transition towards a phase in which the Néel vector of giant and other large loops becomes collinear. This nematic transition is also reflected in the structure factor (insets) which has a smooth pinch point structure above the transition and turns patchy below it. At the lowest temperatures the specific heat is anomalous in that it slightly decreases with increasing temperature. This reflects that temperature enhances the constraints due to entropic interactions.

reflecting the low-temperature behavior of a classical Heisenberg system [Fig. 3(a)]. At low temperatures, the specific heat c_V has a value just below unity. Since $1 - c_V$, as $T \rightarrow 0$, is proportional to the zero modes of the ground-state manifold, this indicates that charge ice is significantly more constrained than the pyrochlore Heisenberg AFM (PHAFM), $J_{ab} = J_{aa} = J_{bb} < 0$, whose extensively degenerate ground state is enumerated by *all* possible fully packed AFM loop realizations connected by $(2N)/4$ zero modes resulting in a specific heat that asymptotes to the lower value of $c_V = 3/4$ [see Ref. [26] and, here, Fig. 5(a)]. A small peak in c_V at $T_0/|J| \approx 0.01$, which sharpens with increasing system size [Fig. 3(b)], suggests a previously unnoticed phase transition, whose nature we now elucidate. Interestingly the low-temperature phase exhibits a specific-heat anomaly in that, below T_0 , the specific heat rises as the temperature decreases.

The static structure factor [Fig. 3(a), insets], is taken as

$$S_{\mathbf{k}} = \left| N^{-1} \sum_{i=1}^N \mathbf{s}_i \exp(i\mathbf{k} \cdot \mathbf{r}_i) \right|^2 \quad (1)$$

and thermally averaged over statistically independent spin configurations for a *single* charge ice realization. It shows the distinctive diffuse scattering and pinch-points associated with dipolar spin correlations on the pyrochlore lattice above T_0 . Below T_0 this pinch-point structure becomes patchy, like that of similarly sized individual charge ice ground states [24]. The pinch-point structure arises because all spins that share the same loop are AFM correlated, which implies power-law spin correlations. This is not unlike the case of the PHAFM where, as already noted, the ground-state manifold consists of *all* possible AFM close-packed loop realizations combining to give a smooth diffuse scattering profile at these system sizes. The patchiness is therefore due to the system falling into a restricted subset of the full PHAFM manifold, which does not self-average at our finite system size. It can be removed by

averaging over several tens of charge ice realizations or by considering larger system sizes.

To reveal the structure of the low- T phase we investigate the one-dimensional (1D) AFM structure factor of the l th loop:

$$S_{\text{AFM},\ell}^{\text{loop}} = \left| \frac{1}{l_\ell} \sum_{i=1}^{l_\ell} (-1)^i \mathbf{s}_i \right|^2, \quad (2)$$

where l_ℓ is its length. When $S_{\text{AFM},\ell}^{\text{loop}} = 1$, the loop has complete AFM correlations, while the orientation of its Néel vector may still fluctuate. Figure 4(a) plots $S_{\text{AFM},\ell}^{\text{loop}}$ for loops of various sizes l_ℓ as a function of temperature. Generally, they develop smoothly as the temperature is reduced, but for the two giant loops, the structure factor jumps up abruptly at T_0 . As a reference, data are also shown for the case of noninteracting loops ($J_{ab} = 0$). Above T_0 , loops of all sizes in the full system behave similarly to noninteracting loops, for which the thermal properties are known analytically through integral transfer methods [27,28], exhibiting a continuous rise in AFM order as the temperature decreases. Indeed, rescaling the temperature axis of the $J_{ab} = 0$ data by the factor 0.8 results in almost perfect overlap with the $J_{ab} \neq 0$ data for $T > T_0$, suggesting the full system is well described in this temperature regime by an ensemble of noninteracting spin chains with the renormalized coupling $\approx 0.8J$.

Inspection of the low-temperature spin configurations reveals that, for $T < T_0$, the Néel vectors of the two giant loops align collinearly, motivating the use of the bulk quadrupolar or nematic order parameter [29]: $\mathbf{Q} = \sum_{i=1}^N \mathbf{Q}_i$, where \mathbf{Q} is a traceless symmetric tensor with components

$$Q_i^{\mu\nu} = s_i^\mu s_i^\nu - \frac{1}{3} \delta^{\mu\nu}. \quad (3)$$

A nonzero $\langle \mathbf{Q} \rangle$ signals breaking of rotational symmetry, but not necessarily of time reversal-symmetry, as $Q_i^{\mu\nu}$ is invariant under spin reversal (which costs very little energy when

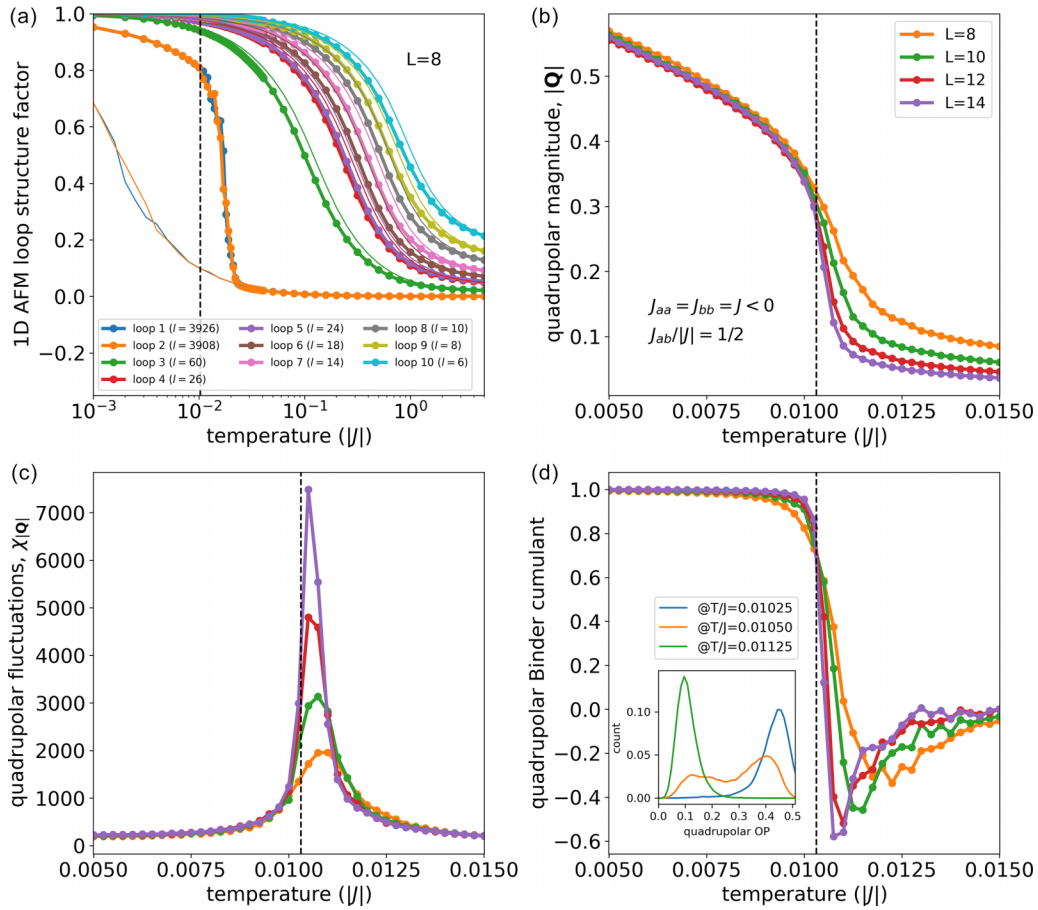


FIG. 4. (a) The one-dimensional AFM loop structure factor as a function of temperature, for different loop sizes in disordered charge ice. Above T_0 all loops exhibit 1D domain wall activity and thus short-range order at a finite temperature, characteristic of Heisenberg spin chains. However, around T_0 , the giant loops show a discontinuous jump in their AFM order as their Néel vectors align. Such alignment is diagnosed (b) by the bulk quadrupolar order parameter \mathbf{Q} whose average magnitude jumps at T_0 concomitant with strong fluctuations, as measured by the generalized quadrupolar susceptibility (c). The first-order nature of this phase transition is revealed by the generalized Binder cumulant [30] which becomes negative close to T_0 indicating a bimodal order-parameter distribution (histograms of $|\mathbf{Q}|$ below, close to, and above T_0 are shown in the inset). In all figures, vertical dashed lines indicate the estimate of the infinite size T_0/J equal to 0.0103, as derived from the Binder cumulant crossing shown in panel (d).

carried out on entire loops). Figures 4(b) and 4(c) plot the average of the magnitude of the quadrupolar order parameter, defined via

$$|\mathbf{Q}|^2 \equiv \text{Tr}[\mathbf{Q}^2], \quad (4)$$

with $|\mathbf{Q}|_{\text{max}}^2 = 2/3$, and a measure of its fluctuations near the transition via the generalized susceptibility,

$$\chi_{|\mathbf{Q}|} = \frac{\langle |\mathbf{Q}|^2 \rangle - \langle |\mathbf{Q}| \rangle^2}{TN}, \quad (5)$$

indicating a rapid, discontinuous turn-on of quadrupolar order that sharpens with increasing system size.

Since \mathbf{Q} and $-\mathbf{Q}$ describe qualitatively different spin structures the Landau free energy does not need to be invariant under a sign change of \mathbf{Q} and will generally contain a cubic term $\text{Tr}(\mathbf{Q}^3)$, ruling out a continuous phase transition. The first-order nature of the transition is indeed confirmed by the generalized Binder cumulant [30] for \mathbf{Q} , which becomes increasingly negative just above T_0 with increasing system size [Fig. 4(d)], due to a bimodal distribution of the

order-parameter magnitude reflecting phase coexistence at T_0 [see inset in Fig. 4(d)]. Together these numerical results indicate that as the temperature is reduced, the magnetic properties may be first characterized by an ensemble of effective one-dimensional Heisenberg spin chains, which via a first-order phase transition nematically align. The origin of the observed alignment and corresponding increase in AFM order in the largest loops will be revealed in a surprisingly accurate mean-field treatment of the transition (see Sec. IV). We now investigate how loop length distribution and loop connectivity affect this phase transition.

B. Role of loop lengths and loop-loop coupling

Figures 5(a) and 5(b) display the heat-capacity and quadrupolar order parameter for a range of $J/|J_{ab}|$ values within region IV. Also shown is the case $J/|J_{ab}| = -1$, which corresponds to the less constrained PHAFM and does not exhibit the nematic transition. Both observables show that T_0 increases as $J/|J_{ab}|$ decreases in magnitude, reaching a maximum around $J/|J_{ab}| = -8/7$ and then decreases,

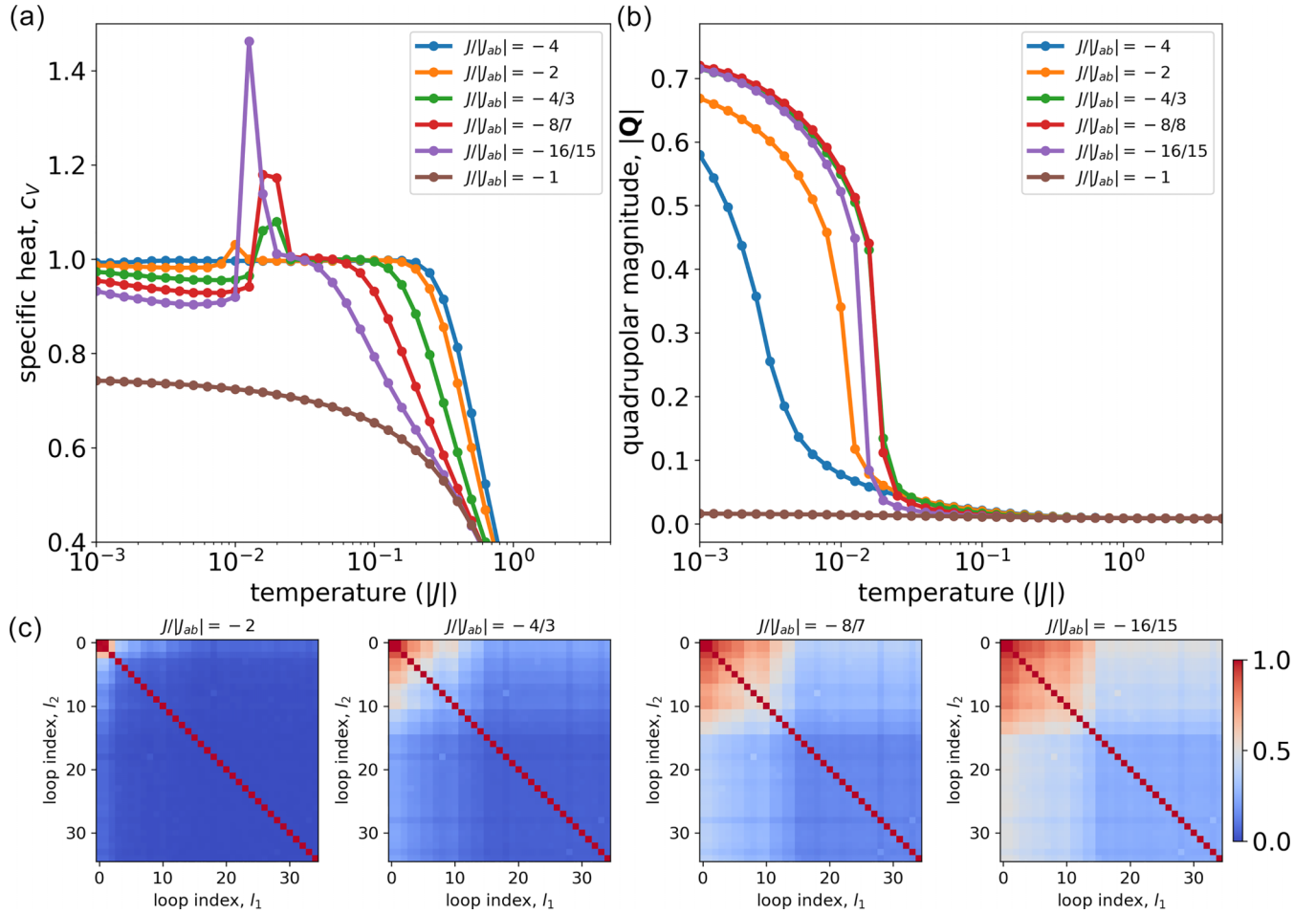


FIG. 5. Thermodynamic quantities of systems with different coupling ratios $J/|J_{ab}|$ within region IV and at its boundary (PHAFM), showing (a) the specific heat and (b) the average quadrupolar magnitude $|\mathbf{Q}|$ as a function of temperature. Except for the PHAFM ($J/|J_{ab}| = -1$), there is a phase transition whose T_0 and heat-capacity signature (latent heat) are controlled by $J/|J_{ab}|$. Data were obtained using an $L = 8$ sample with fixed charge ice structure, containing loops of lengths 3926, 3908, 60, 26, 24, 18 ($2\times$), 14 ($4\times$), 10 ($2\times$), 8 ($2\times$), 6 ($20\times$). (c) Loop-loop quadrupolar correlation matrix using Eq. (6) at the lowest $T/|J| = 0.001$ for different loop couplings. As $J/|J_{ab}|$ approaches -1 from below also smaller loops align increasingly and participate in the phase transition.

indicating nonmonotonic behavior very close to the PHAFM boundary ($J/|J_{ab}| = -1$). The magnitude of $|\mathbf{Q}|$ below T_0 also increases, indicating that a growing fraction of the sample nematically aligns. Defining \mathbf{Q}_l as the quadrupolar order parameter of the l th loop, this trend is reflected in the loop-loop quadrupolar correlation function,

$$\frac{\langle \text{Tr}[\mathbf{Q}_{l_1} \mathbf{Q}_{l_2}] \rangle}{(\langle |\mathbf{Q}_{l_1}|^2 \rangle \langle |\mathbf{Q}_{l_2}|^2 \rangle)^{1/2}}, \quad (6)$$

shown in Fig. 5(c). For $J/|J_{ab}| = -2$ the two giant loops dominate the transition and only their Néel vectors become well aligned. However, as $J/|J_{ab}|$ decreases in magnitude, smaller and smaller loops take part in the alignment and contribute to the bulk quadrupolar order parameter. This trend saturates around $J/|J_{ab}| = -8/7$. Note that even at this optimal coupling for nematic ordering, the smallest loops remain only weakly aligned.

These results might suggest the giant loops are an essential ingredient for the transition to occur, but this turns out not to be the case. In the first instance, the use of open boundary

conditions (not shown) is found to have little effect on the transition as long as sufficiently large loops remain present. We have investigated this conclusion more systematically by performing Monte Carlo (MC) simulations on an $L = 8$ system for which the loop structure generation was biased towards smaller loops. This bias was achieved by only allowing changes in the structure which reduced the sum of the square of loop lengths. In particular, this procedure was applied to the $L = 8$ sample used in the main text, resulting in a sample (referred to as the “small loop” sample) with over 54 loops, the largest ten of which had lengths 1386, 1376, 1236, 1218, 1058, 826, 426, 140, 86, and 30. This should be compared with the original sample which had 35 loops, the largest four of which are 3926, 3908, 60 and 26 in length. Figure 6(a) displays the resulting specific heat compared with the original $L = 8$ charge ice system showing little change in the transition temperature T_0 . Figure 6(b) displays the loop-loop orientation correlation below the critical temperature, demonstrating that the growth in the bulk quadrupolar order parameter is due to the alignment of these larger, but nongiant loops.

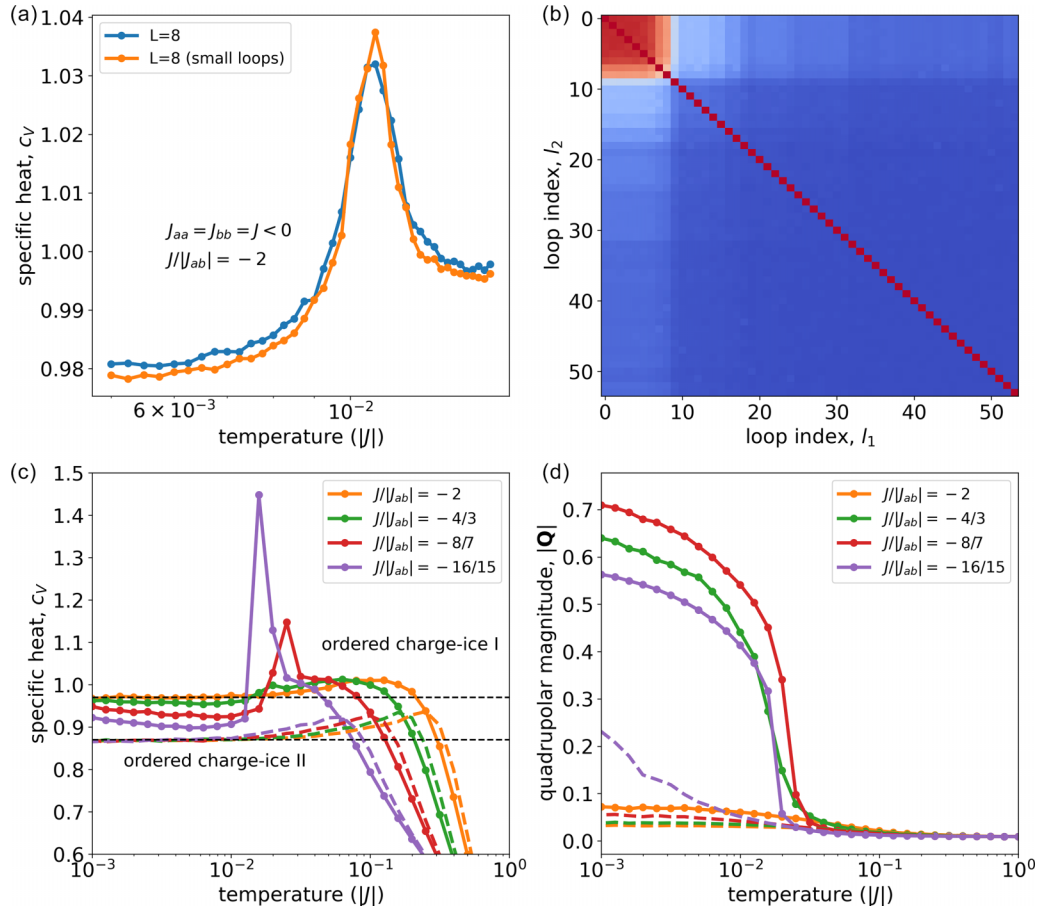


FIG. 6. (a) Heat capacity and (b) loop-loop quadrupolar correlation [Eq. (6)] of an $L = 8$ charge ice system with $J/|J_{ab}| = -2$ in which a bias towards smaller loops has been imposed, eliminating the giant loops. (c) Heat capacity and (d) average quadrupolar magnitude of the ordered charge ice system I (solid lines) and of the ordered charge ice system II (dashed lines) for $L = 8$ and a range of $J/|J_{ab}|$. The dashed black horizontal lines in (c) indicate the value $c_V = 1 - N_{\text{loop}}/N$ expected in the absence of nematic order, which is seen in all cases of charge ice II and in charge ice I for $J/|J_{ab}| = -2$ with $L = 8$.

In Figs. 6(c) and 6(d), we consider the thermodynamics of the two very different *ordered* charge ice systems I and II of size $L = 8$ [for the structures, see Figs. 1(a) and 1(c)]. Both structures are investigated for interchain couplings $J/|J_{ab}|$ equal to -2 , $-4/3$, $-8/7$, $-16/15$. For order of type I with $J/|J_{ab}| = -2$, inspection reveals the absence of the first-order phase transition. However, with increasing interloop coupling, as $J/|J_{ab}|$ becomes less negative, the transition appears, with T_0 again increasing as $J/|J_{ab}|$ approaches -1 , as for the case of the general charge ice structure. For order of type II, instead, we find the phase transition to remain absent for all simulated values of $J/|J_{ab}|$. For both ordered charge ice structures, in the *absence* of a transition the specific-heat plateaus to $1 - N_{\text{loop}}/N$, where N_{loop} is the number of loops and $N = (16L^3)$ is the number of sites. The deviation from 1 reflects the fraction of zero modes in the ground-state manifold [26]. Here their number equals twice the number of loops, while the total number of modes is equal to $2N$. For ordered charge ice I, $N_{\text{loop}} = 4L^2$ and for ordered charge ice II $N_{\text{loop}} = L^2 + 2L^3$ giving the respective specific-heat plateaus of 0.97 and 0.87 [see Fig. 6(c)]. In the presence of ordering the $T = 0$ zero modes experience fluctuational quartic interactions and contribute

$1/4$ to the specific heat. This will, however, be obscured at the probed temperatures by the fluctuations associated with the nematic ordering to be investigated in the proceeding sections.

Together these numerical results demonstrate that whether a first-order phase transition is seen will depend on both the value of $J/|J_{ab}|$ and the distribution of loop lengths within the charge ice structure. We understand this in more depth via the mean-field calculation of the next section.

IV. THEORETICAL ANALYSIS AND DISCUSSION

In this section we demonstrate that nematic alignment originates from maximizing spin entropy and is driven by the phenomenon of order-by-disorder, a mechanism already at play at the level of individual tetrahedra. Based on the ensuing entropic interaction, we develop a mean-field theory for the onset of a symmetry-breaking spin-anisotropy and demonstrate a first-order transition to a nematic phase which is sensitive to loop lengths, temperature and interloop coupling. The predictions of mean-field theory turn out to be remarkably accurate when compared with the numerical results presented in the previous sections.

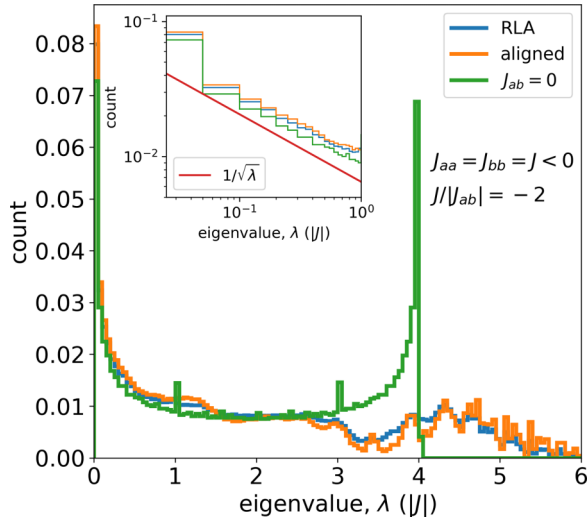


FIG. 7. Density of normal-mode frequencies of the transverse harmonic spin fluctuations around a specific ground-state configuration. Data are shown for both aligned and randomly aligned (RLA) ground-state configurations, respectively. Each loop contributes two zero-modes (not shown). In the low-frequency regime, a power-law $1/\sqrt{\lambda}$ is seen (inset), a fingerprint of fluctuations around 1D long-range-ordered AFM chain configurations.

A. Order-by-disorder and symmetry reduction from Heisenberg to Ising loops

Insight into why the nematic structure is favored at low temperature can be gained from the thermal properties of a single tetrahedron. Expanding the corresponding four-spin Hamiltonian to quadratic order with respect to transverse fluctuations around a ground-state configuration defined by the angle ϕ between the Néel vectors of the two species (see Appendix A), yields a fluctuational entropy,

$$\begin{aligned} \Delta S^{(2)}[\cos^2 \phi] &= -\frac{1}{2} \ln [1 - J_{ab}^2/J^2 \cos^2 \phi] \\ &\approx \frac{1}{2} \frac{J_{ab}^2}{J^2} \cos^2 \phi, \end{aligned} \quad (7)$$

that favors collinear alignment of the Néel vectors, the second expression being valid to lowest order in the interloop couplings J_{ab} . This suggests that the observed first-order transition is driven by an entropic order-by-disorder mechanism [26,31–33], which is already manifest at the tetrahedral level. Such an order-by-disorder phenomenon selects those states purely on entropy grounds. A similar harmonic analysis may be carried out for a ground-state spin configuration of a charge ice realization (in our simulation for a cube of linear size $L = 8$), where now the eigenvectors and corresponding eigenvalues λ of the Hessian M [calculated via Eq. (A4)] are obtained numerically.

Figure 7 displays the normal-mode density of states (DOS) for two ground-state configurations: one with nematic order, in which all loop Néel vectors are aligned; and one where they are randomly oriented with respect to each other (random loop AFM or RLA). These states are both members of the manifold of ground states identified by Banks and Bramwell [24], and are indistinguishable in terms of their internal energies.

The DOS of the RLA depends slightly on the particular ground-state configuration, but for sufficiently large samples self-averaging reduces such differences. For smaller samples an average over many choices of random alignments results in a converged DOS. Both RLA and nematic order reveal $2N_{\text{loop}}$ zero-modes reflecting the $O(3)$ degrees of freedom to choose a Néel vector on each individual loop. While there are differences between the nematic and random ground-state configurations (e.g., the enhanced density of low frequency modes and the more discrete structure at higher frequencies in the nematic ground state), the similarities at low frequency are more revealing. In particular, a log-log plot (inset of Fig. 7) shows in both cases the asymptotic form $\rho(\lambda) \sim 1/\sqrt{\lambda}$ for small λ —a hallmark signature of the fluctuation spectrum of AFM-ordered reference configurations of 1D Heisenberg spin chains. For comparison the DOS derived from the harmonic Hessian with $J_{ab} = 0$ is also shown. Such a system consists of N_{loop} noninteracting finite 1D antiferromagnetic spin chains, whose mode spectrum is known analytically (neglecting finite loop size corrections due to a small fraction of short loops): $\rho(\lambda) \propto \sqrt{\lambda(4J - \lambda)}$.

Within the harmonic approximation, the difference in fluctuational entropy between nematic and RLA states is given by $-\int_{0+}^{\infty} d\lambda [\rho_{\text{nematic}}(\lambda) - \rho_{\text{RLA}}(\lambda)] \ln(\lambda)$ which we find to be a positive quantity. This originates from the coupling-induced softening of low-frequency normal modes, which enhances the $1/\sqrt{\lambda}$ tail, as is seen in the inset of Fig. 7. This softening effect is strongest for the nematically aligned configuration (hence the enhancement at low frequency compared with a randomly aligned ground-state configuration), which is thus entropically favored. Indeed, the fluctuational entropy of nematic order with a finite $Q_z = \langle \cos^2 \phi \rangle - 1/3$ exceeds that of randomly aligned configurations by $\frac{1}{2} Q_z J_{ab}^2/J^2$ per spin [at small coupling $|J_{ab}/J| \ll 1$, see Eq. (14), Sec. IV B], which is comparable to the entropy gain of a single tetrahedron, cf. Eq. (7).

B. Effective Hamiltonian with entropic interactions

The above results yield an effective, entropic interaction between neighboring loops of different cations with their locally AFM correlated configurations. Since the AFM interaction between the loops is frustrated the resulting interaction is comparatively weak. Note that a given loop sees a lot of neighboring loop segments, and thus has a high coordination number. This motivates us to treat the effect of the neighboring loops at the mean-field level, while treating the AFM couplings along the loops exactly. This will result in a mean-field theory for entire loops, with an associated loop-decoupled effective spin Hamiltonian $H = \sum_{\ell} H_{\ell}$.

Let us assume that the temperature is sufficiently low, $T \ll J$, such that AFM correlations are well established at the length-scale of a tetrahedron. In this regime, the spin directions define the local orientation of the AFM structure. We then may approximate the entropy of every tetrahedron as

$$\begin{aligned} \Delta S^{(2)}[(\hat{\mathbf{n}}_a \cdot \hat{\mathbf{n}}_b)^2] &\approx \Delta S \cdot (\hat{\mathbf{n}}_a \cdot \hat{\mathbf{n}}_b)^2 \\ &\approx \frac{\Delta S}{4} \sum_{m,k=1}^2 (\hat{\mathbf{s}}_{a,m} \cdot \hat{\mathbf{s}}_{b,k})^2, \end{aligned} \quad (8)$$

where $\hat{\mathbf{n}}_{a/b}$ is the Néel vector on the loops of type a, b , respectively, $\hat{\mathbf{s}}_{a/b,1}$ and $\hat{\mathbf{s}}_{a/b,2}$ are the two spins on either cation type, and we expanded the effective interaction Eq. (7) to leading order in J_{ab} , with

$$\Delta S = \frac{1}{2} \frac{J_{ab}^2}{J^2}. \quad (9)$$

Using this entropic interaction leads to the effective temperature dependent Hamiltonian

$$H \approx -J \sum_{\ell} \sum_{i \in \ell} \hat{\mathbf{s}}_i \cdot \hat{\mathbf{s}}_{i+1} - \frac{T \Delta S}{4} \frac{1}{2} \sum_i \sum_{j \in \overline{m}(i)} (\hat{\mathbf{s}}_i \cdot \hat{\mathbf{s}}_j)^2, \quad (10)$$

where periodic boundary conditions for the site labels on the closed loops ℓ are assumed, and $\overline{m}(i)$ denotes the i th site's nearest neighbors of opposite cation type.

C. Mean-field theory for loops

We now decouple the individual loops in a mean-field spirit, by considering the presence of an effective symmetry-breaking anisotropy due to an emergent quadrupolar order. We rewrite the interloop couplings $(\hat{\mathbf{s}}_i \cdot \hat{\mathbf{s}}_j)^2 = \sum_{\alpha, \beta} s_{\alpha i} s_{\beta i} s_{\alpha j} s_{\beta j}$ (with $\alpha, \beta \in \{x, y, z\}$) as

$$\begin{aligned} & \sum_{\alpha, \beta} [(s_{\alpha i} s_{\beta i} - \langle s_{\alpha i} s_{\beta i} \rangle)(s_{\alpha j} s_{\beta j} - \langle s_{\alpha j} s_{\beta j} \rangle) \\ & + s_{\alpha i} s_{\beta i} \langle s_{\alpha j} s_{\beta j} \rangle + s_{\alpha j} s_{\beta j} \langle s_{\alpha i} s_{\beta i} \rangle \\ & - \langle s_{\alpha i} s_{\beta i} \rangle \langle s_{\alpha j} s_{\beta j} \rangle]. \end{aligned} \quad (11)$$

We then assume quadrupolar order with polarization axis along z to set in, while preserving rotational symmetry around the z axis. This implies local spin-spin correlations

$$\langle s_{\alpha i} s_{\beta i} \rangle = \delta_{\alpha \beta} \left[\frac{1}{3} + Q_z \left(\frac{3}{2} \delta_{\alpha z} - \frac{1}{2} \right) \right], \quad (12)$$

whose form ensures that the trace of the spin correlator equals one. Note that in general the nematic order parameter depends on the length and cation type of the loop that the site i belongs to. However, in the simplest mean-field only the loop average Q_z enters [cf. Eq. (20) below]. Spin inversion symmetry implies $\langle s_{xi} \rangle = \langle s_{yi} \rangle = \langle s_{zi} \rangle = 0$. Substituting the above into Eq. (11), and dropping the term quadratic in the fluctuations around the mean, finally gives

$$(\hat{\mathbf{s}}_i \cdot \hat{\mathbf{s}}_j)^2 \approx \frac{3}{2} Q_z (s_{zi}^2 - \frac{1}{3} + s_{zj}^2 - \frac{1}{3}) - \frac{3}{2} Q_z^2 + \frac{1}{3}. \quad (13)$$

This mean-field approximation decouples the loops, splitting the Hamiltonian (10) into a sum of loop contributions, $H = \sum_{\ell} H_{\ell}$, with effective loop Hamiltonians (dropping an irrelevant overall additive constant)

$$H_{\ell} = - \sum_{i \in \ell} \left[J \hat{\mathbf{s}}_i \cdot \hat{\mathbf{s}}_{i+1} + AT Q_z \left(s_{zi}^2 - \frac{1}{3} \right) - \frac{1}{2} AT Q_z^2 \right], \quad (14)$$

with

$$A \equiv \frac{3}{2} \Delta S = \frac{3}{4} \frac{J_{ab}^2}{J^2}. \quad (15)$$

As all loops have even length we can perform a simple gauge transformation $s_i \rightarrow (-1)^i s_i$ to switch from AFM ($J < 0$) to FM interactions ($J' = |J| > 0$) in Eq. (10). The free energy

$F_{\text{MF}}(L; Q_z)$ of a loop of length L can be found with transfer-matrix methods. In the limit of large correlation lengths, $T \ll |J|$, one may resort to a continuum spin field approximation [34], which yields the expression

$$\beta F_{\text{MF}}(L; Q_z) = - \ln [\text{Tr}(\exp(-\beta \mathcal{H}L))], \quad (16)$$

where the operator

$$\mathcal{H} = \Delta E + \frac{T^2}{2|J|} \tilde{L}^2 - AT Q_z \left(\cos^2 \theta - \frac{1}{3} \right) + \frac{AT Q_z^2}{2} \quad (17)$$

is the quantum-mechanical hindered rotor Hamiltonian, \tilde{L} being the angular-momentum operator in spherical coordinates (ϕ, θ) . This result has its origin in the equivalence between the transfer-matrix eigenvalue method used to evaluate the functional integrals of 1D classical statistical mechanics, and the zero-dimensional single-particle quantum mechanical problem. In the above, the Q_z -independent term

$$\Delta E = -|J| + T \ln(|J|/T) \quad (18)$$

is the free-energy density of an infinite Heisenberg chain with periodic boundary conditions. The trace in Eq. (16) is over the square integrable functions on the sphere.

The total free energy per site within this mean-field approximation follows as

$$f_{\text{MF}}(Q_z) = \frac{1}{N} \sum_{\ell} F_{\text{MF}}(L_{\ell}; Q_z), \quad (19)$$

where N is the number of sites and L_{ℓ} is the length of loop ℓ . The self-consistency condition on Q_z reads

$$\begin{aligned} Q_z &= \frac{1}{N} \sum_{\ell} L_{\ell} (\cos^2(\theta) - 1/3)_{L_{\ell}; Q_z}, \\ \langle O \rangle_{L; Q_z} &\equiv \frac{\text{Tr}(O \exp(-\beta \mathcal{H}L))}{\text{Tr}(\exp(-\beta \mathcal{H}L))}, \end{aligned} \quad (20)$$

which, as usual, is equivalent to imposing a (local) minimum of the constrained mean-field free energy, $\partial f_{\text{MF}} / \partial Q_z = 0$. The equilibrium configuration corresponds to the global minimum of $f_{\text{MF}}(Q_z)$.

Below we exploit this general formalism in two limits: (i) the limit $T \rightarrow 0$, where the transverse fluctuations on a given loop become irrelevant and the only remaining degree of freedom is the Néel vector of a loop ℓ ; and (ii) the case where essentially all loops in the considered charge ice are large, $L_{\ell} \gg 1$ (more precisely $L_{\ell} \gg T/\delta E$, where δE is the spectral gap of \mathcal{H}), in which case the free energy per site is given by the lowest eigenvalue of \mathcal{H} . This simplifies our analytical study of the finite-temperature behavior.

D. Nematic transition in the limit $T \rightarrow 0$

We first investigate the possibility of loop alignment at very low temperature T , such that the correlation length $L_T = J/T$ of a Heisenberg chain exceeds the length of any given loop ℓ . We have in mind the analysis of charge ice structures with relatively short loops, for which we aim to show that a minimal coupling strength J_{ab} is needed to induce ordering.

In this low-temperature regime, the spin chain on the loop ℓ is well characterized by its Néel vector \mathbf{n}_{ℓ} , which is the only relevant degree of freedom left. For its z component we write

$n_z \equiv \cos(\theta)$. The angular-momentum part of \mathcal{H} in Eq. (17), which captures spin-wave fluctuations, becomes irrelevant for $T \rightarrow 0$ and the loop free energy (16) reduces to

$$\beta(F_{\text{MF}}(L; Q_z) - \Delta EL) = -\ln \left[\int_{-1}^1 dn_z \exp \{AL[Q_z(n_z^2 - 1/3) - Q_z^2/2]\} \right], \quad (21)$$

where we split off the Q_z -independent term ΔE from the free energy.

1. Charge ice with loops of equal, finite length

As a specific example, we consider a periodic charge-ordered system of finite size L , which contains $N_l = 4L^2$ loops of length $l = 4L$, where each loop shares at most one tetrahedron with any other loop—the ordered charge ice I structure [Fig. 1(a)].

Let us now determine whether it is consistent to assume that $Q_z = \langle n_z^2 \rangle - 1/3$ acquires a finite expectation value, and thus spontaneously breaks the rotational invariance. Self-consistency of the mean-field requires that

$$Q_z = \frac{\int_{-1}^1 dn_z \exp [AlQ_z(n_z^2 - 1/3)](n_z^2 - 1/3)}{\int_{-1}^1 dn_z \exp [AlQ_z(n_z^2 - 1/3)]}. \quad (22)$$

For large Al the integral is dominated by $n_z = \pm 1$ and there is a nontrivial solution with $Q_z \approx 2/3$. However, this symmetry-breaking solution disappears at the spinodal point $Al \approx 10.1 \equiv (Al)_{\text{sp}}^{(1)}$, where the order parameter discontinuously drops from $Q_z \approx 0.205$ to zero, signaling a first-order transition. This is consistent with the fact that nematic transitions cannot be continuous, as we discussed in Sec. III A. The disordered phase ($Q_z = 0$) displays a similar spinodal instability at $(Al)_{\text{sp}}^{(2)} = 45/4 = 11.25$ beyond which the disordered solution $Q_z = 0$ is locally unstable. The equilibrium transition between the disordered and the symmetry broken solution takes place where the two associated free energies cross. This happens at $Al = (Al)_0 \approx 10.218$, where the order parameter jumps to the finite value $Q_z \approx 0.286$.

In charge ice systems with equally long loops low-temperature order is thus predicted to exist only if the loop length exceeds

$$l_0 = \frac{(Al)_0}{A} = \frac{4(Al)_0}{3} \frac{J^2}{J_{ab}^2} = 13.6 \frac{J^2}{J_{ab}^2}, \quad (23)$$

which scales inversely with the entropy gain $\Delta S \sim (J_{ab}/J)^2$ for alignment. Indeed, for loops longer than l_0 , the entropy gain $l\Delta S^{(2)}\Delta Q_z$ ($\Delta Q_z \approx 0.28$) from (partial) alignment can compensate the entropy $O(1)$ lost due to constraining the loop's Néel vector.

For the case of our ordered finite-size charge ice where $l = 4L$, the nematic phase transition will only occur for periodic samples of size L , when $J_{ab}/|J| > J_{ab}^0/|J| = [4(Al)_0/3l]^{1/2} = [(Al)_0/3L]^{1/2}$. For the case of $L = 8$ this requires $J_{ab}/J > 0.65$ or $J/|J_{ab}| < -1.53$. Considering finite-size ordered charge ices at $T = 0^+$, nematic order emerges discontinuously as the loops reach the critical length $l = l_0$. The nematic order is absent in charge ice structures with too short loops and/or too weak interloop couplings, as seen in the data of Figs. 5, 6(a), and 6(b).

The above analysis shows that short loops resist nematic ordering. In an ordered structure containing alternating short loops and (winding) large loops, one still expects order in the thermodynamic limit. However, the nematic transition temperature will be substantially reduced due to the strong fluctuations of the small loops, which only mediate a very weak coupling between the long loops. This is indeed the case for the ordered charge ice system II [Fig. 1(d)] where the finite-size systems of Figs. 6(c) and 6(d) show *no* signature of the nematic transition.

2. Charge ice with distributed loop sizes

It is not difficult to generalize the analysis to a charge ice configuration with an ensemble of loops with a distribution of lengths. We assume normalized loop length distributions $P_{a/b}(l)$ for loops of cation type a and b . We further assume an absence of loop-loop correlations. Namely when considering a given loop of type a , we assume that $lP_b(l)$ represents the probability of it sharing a tetrahedron with a b type loop of length l , independently of the length of the considered a loop. We then can evaluate the average quadrupolar field component for sites of type a/b as

$$\bar{Q}_z^{a/b} = \frac{\sum_l lP_{a/b}(l)Q_z^{a/b}(l)}{\sum_l lP_{a/b}(l)}, \quad (24)$$

where

$$Q_z^{a/b}(l) = \frac{\int_{-1}^1 dn_z \exp [lA\bar{Q}_z^{b/a}(n_z^2 - 1/3)](n_z^2 - 1/3)}{\int_{-1}^1 dn_z \exp [lA\bar{Q}_z^{b/a}(n_z^2 - 1/3)]}. \quad (25)$$

Here $Q_z^{a/b}(l)$ is the quadrupolar order parameter that establishes on loops of length l of type a/b . In a slight generalization of the above mean-field approach, we allow for the possibility of (slightly) different order parameters $Q_z^{a/b}$, which represent the average of the nematic order over loops of one cation type only.

By using the loop length distribution of a simulated charge ice structure, the self-consistent solution entailed by Eqs. (24) and (25) may be compared with that found by the MC numerics. Indeed, the average order parameter $\bar{Q}_z^{a/b}$ and Eq. (25) may be used to calculate the orientational correlation between two loops, $\langle \text{Tr}[\mathbf{Q}_{l_1} \mathbf{Q}_{l_2}] \rangle / (\langle |\mathbf{Q}_{l_1}|^2 \rangle \langle |\mathbf{Q}_{l_2}|^2 \rangle)^{1/2}$, for example for the charge ice realization shown in Fig. 5. We take l_1 to be a giant loop of type a/b whose quadrupolar field is oriented along $\hat{\mathbf{z}}$ with magnitude very close to $\bar{Q}_z^{a/b}$, while l_2 is a small loop of type b/a . Figure 8 compares this correlation to the simulated data of Fig. 5(c) showing very good agreement. This quantitatively confirms the initial assumption entailed in Eq. (10) and the general mean-field approach. For this system $\bar{Q}_z^a/(2/3) = 0.983$ and $\bar{Q}_z^b/(2/3) = 0.971$ reflecting the small fraction of sites that belong to small loops $[1 - Q_z/(2/3)]$.

Our analysis shows that the existence of the nematic phase and the value of T_0 both hinge on the distribution of loop lengths and the connectivity among the loops of different sizes. The stronger the interloop coupling, the more small loops align significantly with the global nematic order parameter. For a given interloop coupling, the magnitude of $1 - Q_z/(2/3)$ in random charge ice structures can be taken as a measure of the fraction of sites belonging to small loops.

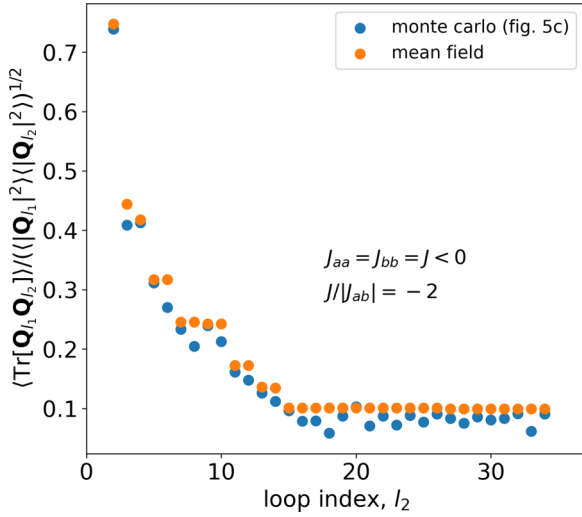


FIG. 8. Mean-field prediction of loop-loop quadrupolar correlation for small loops (l_2) embedded in the quadrupolar field of larger loops. Here we take l_1 to be a giant loop. This is to be compared with low temperature $T/|J| = 0.001$ Monte Carlo simulations of the $L = 8$ charge ice realization of Fig. 5(c) for the case of $J/|J_{ab}| = -2$.

E. Finite-temperature transition in charge ice with large loops

Let us now analyze the case of charge ices in which (almost) all loops are large. This is a reasonable approximation for random charge ice, where small loops are relatively rare. In this case the trace in Eq. (16) is dominated by the ground-state energy ϵ_0 of \mathcal{H} in Eq. (17),

$$f_{\text{MF}}[Q_z] = \lim_{L \rightarrow \infty} \frac{F_{\text{MF}}[L, Q_z]}{L} = \epsilon_0[\mathcal{H}]. \quad (26)$$

Introducing the reduced temperature $\tau \equiv T/|J|A$, it is convenient to rewrite this as

$$\frac{f_{\text{MF}}[Q_z] - \Delta E}{|J|A^2} = \tau^2 \tilde{\epsilon}_0[\tilde{\mathcal{H}}[Q_z/\tau]] + \frac{\tau}{2} Q_z^2, \quad (27)$$

with the reduced hindered rotor Hamiltonian $\tilde{\mathcal{H}}$,

$$\tilde{\mathcal{H}}[Q_z/\tau] = \frac{\tilde{L}^2}{2} - \frac{Q_z}{\tau} \left(\cos^2(\theta) - \frac{1}{3} \right). \quad (28)$$

It remains to minimize the mean-field free energy (27) with respect to the order parameter Q_z . Second-order perturbation theory assures that $\tilde{\epsilon}_0 \sim Q_z^2$ for small Q_z , and thus, a local extremum at $Q_z = 0$ always exist. However, the coefficient of the quadratic term changes sign at low temperature ($\tau_{\text{sp}}^{(2)} = 8/135 \approx 0.593$), rendering this disordered minimum unstable. However, before this happens, a secondary minimum at a finite Q_z emerges and drops below $f_{\text{MF}}(Q_z = 0) = \Delta E$, indicating a first-order transition.

The transition happens when, for a positive Q_z , one finds simultaneous solutions of $f_{\text{MF}} = \Delta E$ and $df_{\text{MF}}/dQ_z = 0$, or

$$\tau^2 \tilde{\epsilon}_0 \left(\frac{Q_z}{\tau} \right) + \frac{1}{2} \tau Q_z^2 = 0, \quad (29)$$

$$\tau \tilde{\epsilon}'_0 \left(\frac{Q_z}{\tau} \right) + \tau Q_z = 0, \quad (30)$$

where we consider $\tilde{\epsilon}_0[\tilde{\mathcal{H}}] = \tilde{\epsilon}_0(Q_z/\tau)$ as a function of the coefficient Q_z/τ in Eq. (28).

Multiplying the second equation by $Q_z/2$ we find for $\rho = Q_z/\tau$ the equation

$$\tilde{\epsilon}_0(\rho) = \frac{\rho}{2} \tilde{\epsilon}'_0(\rho). \quad (31)$$

From its solution, ρ^* , one obtains the order parameter at the first-order transition,

$$Q_z^* = -\tilde{\epsilon}'_0[\rho^*], \quad (32)$$

and the transition temperature

$$\frac{T_0}{A|J|} = \tau^* = \frac{Q_z^*}{\rho^*}. \quad (33)$$

Carrying out this procedure numerically, one finds

$$\rho^* = 3.5569, \quad (34)$$

$$Q_z^* = 0.2377, \quad (35)$$

$$\tau^* = 0.0668. \quad (36)$$

This predicts the equilibrium first-order transition to take place at the temperature

$$\frac{T_0}{|J|} = A\tau^* = 0.100\Delta S. \quad (37)$$

In our derivation we have assumed that all loops are large and thus contribute essentially equally to the symmetry-breaking quadrupolar field. This is, however, not entirely true in typical charge ice samples, since the loops smaller than a certain length threshold do not actively participate in the transition. To a first approximation this can be taken into account by assuming that only an average fraction $c < 1$ of the sites neighboring a given loop belong to loops above a certain length threshold. This then modifies Eq. (37) to

$$\frac{T_0}{|J|} = 0.100c\Delta S = 0.050c \left(\frac{J_{ab}}{J} \right)^2. \quad (38)$$

This rationalizes the observed temperature scale of T_0 and its decrease as $J/|J_{ab}|$ becomes more negative. Indeed, for $J/|J_{ab}| = -2$ the mean-field prediction gives $T_0 = 0.0125c$. The fraction c depends on the microstructure of the charge ice, in particular on its loop distribution function, an aspect already encountered in the previous section. The mean-field prediction is remarkably close to that of simulation (Fig. 4) for a value $c \approx 0.95$ which, for charge ice, is the approximate fraction of sites involved in loops longer than the critical length l_0 defined in Sec. IV D.

F. Specific heat in charge ice at $T \ll T_0$

Mean-field theory also explains the unusual temperature dependence of the specific heat in the nematic phase [Fig. 3(a)]. The specific heat can be evaluated via

$$c_V = -T \frac{\partial^2}{\partial T^2} f_{\text{MF}} = -\frac{\tau}{A|J|} \frac{\partial^2}{\partial \tau^2} f_{\text{MF}}. \quad (39)$$

The Q_z independent part ΔE of the free energy contributes $c_V^0 = -T \frac{\partial^2}{\partial T^2} \Delta E = 1$, as expected from the equipartition theorem. We now show that the entropic interaction introduces a negative correction to this value. Using Eq. (27) together with Eq. (30), the full specific heat evaluates to

$$c_V - c_V^0 = A\tau \left(-2\tilde{\epsilon}_0(Q_z/\tau) - 2\frac{Q_z^2}{\tau} - Q_z Q_z' \right). \quad (40)$$

To proceed we need the asymptotics of $\tilde{\epsilon}_0$ at large argument. This can be obtained, e.g., by calculating the low-temperature free energy of the spin chain via a quadratic expansion with respect to transverse spin fluctuations around a bulk AFM spin configuration aligned along the z axis. This yields

$$\tilde{\epsilon}_0(\rho \equiv Q_z/\tau \gg 1) = -\frac{2}{3}\rho + \sqrt{2\rho} + O(1). \quad (41)$$

This result, based on the continuum approximation, does not include the effect of Z_2 domain walls though. However, as those are exponentially rare they contribute only negligibly to the low-temperature specific heat.

Using the asymptotics (41) in Eq. (30), one obtains the leading temperature dependence of the quadrupolar field as

$$Q_z(\tau \ll 1) \approx \frac{2}{3} - \frac{\sqrt{3\tau}}{2}, \quad (42)$$

which reflects the weakening of nematic order by spin-wave fluctuations. Substitution of these asymptotics into Eq. (40) finally gives

$$c_V \approx 1 - \frac{\sqrt{3}}{2} A\sqrt{\tau} = 1 - \frac{3}{4} \frac{|J_{ab}|}{|J|} \sqrt{\frac{T}{|J|}}. \quad (43)$$

Thus, in the nematic phase at $T \ll T_0$, the specific heat decreases from unity as the temperature increases. This anomalous effect in the specific-heat arises from the quenching of long-wavelength spin waves due to the linear in T increase of the anisotropic quadrupolar field, $\approx T \Delta S$ in Eq. (14), which reflects its entropic origin.

Figure 9 displays the low-temperature regime below the transition and the prediction of Eq. (43), showing good agreement for the case $J/|J_{ab}| = -2$, which is within the assumed perturbative regime. The present calculation does not include the temperature dependent features of the specific heat associated with the release of latent heat close to T_0 , nor does it take into account that in the limit $T \rightarrow 0$, $c_V \rightarrow 1 - \frac{1}{2} N_{\text{loop}}/N$ due to the presence of $2N_{\text{loop}}$ zero modes [26]. Note that the factor of one-half originates from the fact that soft modes only experience effective quartic potentials associated with the entropic quadrupolar interaction, contributing only $k_B/4$ instead of $k_B/2$ to the specific heat. For the charge ice structure $N_{\text{loop}}/N \approx 0.004\text{--}0.005$ —a number that does not depend strongly on the charge ice realization.

V. CONCLUDING REMARKS

While discontinuous transitions were found in related frustrated systems upon homogeneously perturbing the interactions and thereby lifting the ground-state degeneracy [35–38], those are driven by the essentially local competition between

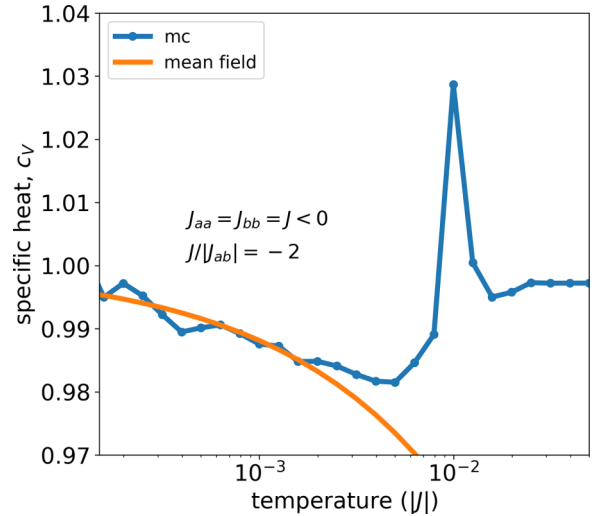


FIG. 9. Low-temperature specific heat as a function of temperature for the case of $J/|J_{ab}| = -2$, along with the mean-field prediction for the nematic phase, cf. Eq. (43).

energy and entropy. In contrast, charge ice establishes a complex connectivity among strongly correlated nonlocal cluster degrees of freedom, which reflect the precise realization of the correlated disorder—and it is with respect to these degrees of freedom that the first-order transition takes place.

The predicted spin nematic breaks spin rotation symmetry, but preserves (statistical) lattice symmetries. It is thus quite distinct from lattice nematics, that break lattice rotation invariance at the level of the spin-spin correlation function [39,40].

The nematic s_z^2 anisotropy below T_0 does not break time-reversal symmetry and no long-range spin order is expected within the nematic phase. However, such a spontaneously emerging anisotropy reduces the $O(3)$ global symmetry of the Heisenberg Hamiltonian to an Ising Z_2 symmetry, which remains unbroken on the chains in accord with the Mermin-Wagner theorem [41]. Thus, above T_0 , loops fluctuate and equilibrate rapidly due to long wavelength spin waves, whereas below T_0 the reduced spin symmetry entails a many orders of magnitude longer spin relaxation time due to the tiny Gibbs factor $\exp(-4J/T)$ associated with the nucleation and separation of a pair of Ising domain-walls. With such kinetics nearly frozen out, the loops maintain their nearly perfect AFM order for very long times, with spin-relaxation times of order $\tau_1 \sim \exp(4J/T)$. This is why a rapid increase in AFM order is seen in the numerics for the largest loops at T_0 [Fig. 4(a)].

Such a spin-liquid freezing, in which sufficiently large loops fall out of equilibrium and become AFM ordered on mesoscopic timescales, differs strongly from the effect of random couplings, which may induce glassy spin freezing [42], with slow dynamics deriving from a complex energy landscape, but occurring at temperatures far below the dominant exchange energy scale.

Our work shows that correlated structural disorder can produce nontrivial behavior due to the emergence of non-local degrees of freedom tied to lower-dimensional clusters (loops or strings). Solids in which similarly correlated disorder is known (or expected) to exist are numerous [20,43,44], with corner-sharing tetrahedra being only one example of

a more general class of materials whose corner or edge-sharing plaquettes may show qualitatively different magnetic behavior [33,45,46]. Moreover, transferring the paradigm of nonlocal, intertwined degrees of freedom that arise from correlated disorder to the realm of continuous phase transitions might offer the possibility of entirely new universality classes [47]. In the present system, such a phenomenon might be realized or tuned-to through an appropriate external field or heterogeneous strain.

Quantitatively understanding the relation between such correlated structural disorder and emergent collective degrees of freedom and their thermodynamic signatures is a formidable but not intractable problem. Indeed, experimentally observing the predicted nematic phase transition through magnetic birefringence would give indirect evidence for the existence of large loops and the presence of correlated disorder. Moreover, if it is possible to vary the exchange constants either chemically or through a global distortion, or alternatively modify the charge ice structure through specific annealing protocols, and monitor the transition temperature and the order-parameter magnitude, one might extract additional information on the distribution of loop lengths, establishing an experimental link between correlated disorder and the thermodynamics it entails.

ACKNOWLEDGMENTS

The authors wish to thank Sam Garratt, Afonso Dos Santos Rufino, and Hugo Bocquet for helpful discussions. We also thank Christian Rüegg for doctoral supervision of A.H. The work was partly supported by the European Union Horizon 2020 research and innovation program under the Marie Skłodowska-Curie Grant Agreement No. 884104 (PSI-FELLOW-III-3i) and the Swiss National Science Foundation (Grants No. 200020_182536 and No. 200020_200558).

P.M.D. and T.F. instigated the project; A.H., P.M.D., K.E., and M.T. performed the simulations; A.H., K.E., T.F., and P.M.D. carried out the analyses; P.M.D. and M.M. carried out the theoretical calculations; P.M.D., T.F., and M.M. wrote the paper with input from the other authors.

APPENDIX A: HARMONIC TRANSVERSE SPIN FLUCTUATIONS FOR A SINGLE TETRAHEDRON

The classical Heisenberg spin Hamiltonian may be written as

$$H = -\frac{1}{2} \sum_{ij} J_{ij} \hat{\mathbf{s}}_i \cdot \hat{\mathbf{s}}_j, \quad (\text{A1})$$

for which the local field at each site i is

$$\mathbf{b}_i = \sum_j J_{ij} \hat{\mathbf{s}}_j. \quad (\text{A2})$$

To investigate the transverse spin fluctuations, $\mathbf{s}_{\perp,i}$ with respect to a given spin configuration $\hat{\mathbf{s}}_{0,i}$ each spin is written as

$$\hat{\mathbf{s}}_i = \mathbf{s}_{\perp,i} + \hat{\mathbf{s}}_{0,i} |\mathbf{s}_{\parallel,i}|, \quad (\text{A3})$$

where $|\mathbf{s}_{\parallel,i}| = (1 - |\mathbf{s}_{\perp,i}|^2)^{1/2}$. If the magnetic configuration $\hat{\mathbf{s}}_{0,i}$ is at a local energy minimum then all $\hat{\mathbf{s}}_{0,i}$ will be parallel to

their local fields, $\mathbf{b}_{0,i}$. Then to quadratic order in the transverse components, the Hamiltonian may be written as $H = H^{(0)} + \Delta H^{(2)}$, where

$$\begin{aligned} \Delta H^{(2)} &= -\frac{1}{2} \sum_{ij} (J_{ij} - |\mathbf{b}_{0,i}| \delta_{i,j}) \mathbf{s}_{\perp,i} \cdot \mathbf{s}_{\perp,j} \\ &= -\frac{1}{2} \sum_{ij} \Lambda_{ij} \mathbf{s}_{\perp,i} \cdot \mathbf{s}_{\perp,j}. \end{aligned} \quad (\text{A4})$$

In the above, the off-diagonal term J_{ij} is the full three-dimensional (3D) Hessian whereas the second diagonal term is a correction to the 3D Hessian which projects the taken derivatives onto the tangent space of each spin.

Representing the two-dimensional (2D) tangent space of spin i as $\mathbf{e}_{1,i}$ and $\mathbf{e}_{2,i}$ with $\mathbf{e}_{1,i} \times \mathbf{e}_{2,i} = \hat{\mathbf{s}}_{0,i}$, the transverse fluctuations of the i th spin may be written as

$$\mathbf{s}_{\perp,i} = \sum_{\alpha=1,2} \chi^{\alpha,i} \mathbf{e}_{\alpha,i}, \quad (\text{A5})$$

where $\chi^{\alpha,i}$ are (small) real numbers. The choice of the $\mathbf{e}_{\alpha,i}$ is not unique and we follow Ref. [48]. Together the above yields a symmetric matrix $M_{i\alpha,j\beta}$ of rank $2N$, represented as an $N \times N$ matrix of 2×2 block elements, whose (i, j) th block element is $\Lambda_{ij} \mathbf{e}_{\alpha,i} \cdot \mathbf{e}_{\beta,j}$. Solving the corresponding eigenvalue-problem yields the normal modes of Eq. (A4) that govern the fluctuations of this quadratic Hamiltonian. Note that for disordered or frustrated systems, $\hat{\mathbf{s}}_{0,i}$ and thus the local tangent space, defined via $\mathbf{e}_{\alpha,i}$, will be different for each spin. Thus the normal modes presently calculated are nontrivially related to the corresponding spin-wave modes which arise from a linearization of the Landau-Lifshitz equation.

At the level of the quadratic approximation to the Hamiltonian, the resulting partition function becomes a simple Gaussian integral, evaluating to

$$Z = \prod_{n|\lambda_n>0} \sqrt{\frac{2\pi T}{\lambda_n}}, \quad (\text{A6})$$

where the λ_n are the nonzero eigenvalues of the fluctuation matrix M , from which the free energy may be calculated as $F = -T \ln Z$, giving

$$F = \frac{T}{2} \sum_{n|\lambda_n>0} \ln \frac{\lambda_n}{2\pi T}. \quad (\text{A7})$$

In the thermodynamic limit this can be evaluated as an integral $\int_{0^+}^{\infty} d\lambda \rho(\lambda) \ln \lambda$, using the density of eigenvalues (or density of states DOS), $\rho(\lambda)$, which is normalized to $2N$.

The Hamiltonian for a single tetrahedron satisfying the charge ice rule is given by

$$\begin{aligned} H &= -J_{aa} \hat{\mathbf{s}}_{a,1} \cdot \hat{\mathbf{s}}_{a,2} - J_{bb} \hat{\mathbf{s}}_{b,1} \cdot \hat{\mathbf{s}}_{b,2} \\ &\quad - J_{ab} [(\hat{\mathbf{s}}_{a,1} + \hat{\mathbf{s}}_{a,2}) \cdot (\hat{\mathbf{s}}_{b,1} + \hat{\mathbf{s}}_{b,2})], \end{aligned} \quad (\text{A8})$$

where we recall that we focus on the parameter regime where the couplings J_{aa} and J_{bb} are negative (AFM). For a ground-state configuration of region IV, we have the AFM configurations between spins of the same type: $\hat{\mathbf{s}}_{a,1} = -\hat{\mathbf{s}}_{a,2}$ and $\hat{\mathbf{s}}_{b,1} = -\hat{\mathbf{s}}_{b,2}$, and an angle ϕ between the alignment axis. This gives the ground-state energy $-J_{aa} - J_{bb}$, independent of

ϕ . The quadratic Hamiltonian is represented as a matrix of rank eight:

$$M_{i\alpha,j\beta} = \begin{bmatrix} |J_{aa}| & 0 & -J_{aa} & 0 & -J_{ab} & 0 & -J_{ab} & 0 \\ 0 & |J_{aa}| & 0 & J_{aa} & 0 & -J_{ab} \cos \phi & 0 & J_{ab} \cos \phi \\ -J_{aa} & 0 & |J_{aa}| & 0 & -J_{ab} & 0 & -J_{ab} & 0 \\ 0 & J_{aa} & 0 & |J_{aa}| & 0 & J_{ab} \cos \phi & 0 & -J_{ab} \cos \phi \\ -J_{ab} & 0 & -J_{ab} & 0 & |J_{bb}| & 0 & -J_{bb} & 0 \\ 0 & -J_{ab} \cos \phi & 0 & J_{ab} \cos \phi & 0 & |J_{bb}| & 0 & J_{bb} \\ -J_{ab} & 0 & -J_{ab} & 0 & -J_{bb} & 0 & |J_{bb}| & 0 \\ 0 & J_{ab} \cos \phi & 0 & -J_{ab} \cos \phi & 0 & J_{bb} & 0 & |J_{bb}| \end{bmatrix}, \quad (\text{A9})$$

whose four nonzero eigenvalues give the free-energy contribution

$$\Delta F^{(2)}[T, \phi] = \frac{T}{2} \ln \left[\frac{(J_{aa}J_{bb} - J_{ab}^2)(J_{aa}J_{bb} - J_{ab}^2 \cos^2 \phi)}{\pi^4 T^4} \right].$$

The above can be conveniently written as

$$\Delta F^{(2)}[T, \phi] = \Delta F^{(2)}[T] - T \Delta S^{(2)}[\cos^2 \phi], \quad (\text{A10})$$

where (with $k_B = 1$)

$$\Delta S^{(2)}[\cos^2 \phi] = -\frac{1}{2} \ln \left[1 - \frac{J_{ab}^2 \cos^2 \phi}{J_{aa}J_{bb}} \right] \approx \frac{1}{2} \frac{J_{ab}^2}{J_{aa}J_{bb}} \cos^2 \phi \quad (\text{A11})$$

is the (temperature independent) fluctuational entropy evaluated for a given angle ϕ between the orientations of the two equal species pairs, and the last approximation holds for small J_{ab} . Thus the angle-constrained free energy has minima

at $\phi = 0, \pi$ and maxima at $\phi = \pm\pi/2$. Alignment or anti-alignment thus results in maximal fluctuational entropy, that can be quantified by $\Delta S^{(2)}(\phi = 0) - \langle \Delta S^{(2)}(\phi) \rangle_\phi \approx 0.1$ for $J_{ab}/\sqrt{J_{aa}J_{bb}} = 1/2$.

-
- [1] G. Blatter, M. V. Feigel'man, V. B. Geshkenbein, A. I. Larkin, and V. M. Vinokur, Vortices in high-temperature superconductors, *Rev. Mod. Phys.* **66**, 1125 (1994).
- [2] M. Morin, E. Canévet, A. Raynaud, M. Bartkowiak, D. Sheptyakov, V. Ban, M. Kenzelmann, E. Pomjakushina, K. Conder, and M. Medarde, Tuning magnetic spirals beyond room temperature with chemical disorder, *Nat. Commun.* **7**, 13758 (2016).
- [3] A. Scaramucci, H. Shinaoka, M. V. Mostovoy, R. Lin, Ch. Mudry, and M. Müller, Spiral order from orientationally correlated random bonds in classical XY models, *Phys. Rev. Res.* **2**, 013273 (2020).
- [4] A. R. Overy, A. B. Cairns, M. J. Cliffe, A. Simonov, M. G. Tucker, and A. L. Goodwin, Design of crystal-like aperiodic solids with selective disorder-phonon coupling, *Nat. Commun.* **7**, 10445 (2016).
- [5] K. Binder and A. P. Young, Spin-glasses—experimental facts, theoretical concepts, and open questions, *Rev. Mod. Phys.* **58**, 801 (1986).
- [6] C. L. Henley, The “Coulomb phase” in frustrated systems, *Annu. Rev. Condens. Matter Phys.* **1**, 179 (2010).
- [7] J. D. Bernal and R. H. Fowler, A theory of water and ionic solution, with particular reference to hydrogen and hydroxyl ions, *J. Chem. Phys.* **1**, 515 (1933).
- [8] L. Pauling, The Structure and entropy of ice and of other crystals with some randomness of atomic arrangement, *J. Am. Chem. Soc.* **57**, 2680 (1935).
- [9] R. J. Baxter, *Exactly solved models in statistical mechanics* (Academic Press, London, 1982).
- [10] F. Rys, Über ein zweidimensionales klassisches Konfigurationsmodell, *Helv. Phys. Acta* **36**, 537 (1963).
- [11] M. J. Harris, S. T. Bramwell, D. F. McMorrow, T. Zeiske, and K. W. Godfrey, Geometrical frustration in the ferromagnetic pyrochlore $\text{Ho}_2\text{Ti}_2\text{O}_7$, *Phys. Rev. Lett.* **79**, 2554 (1997).
- [12] M. J. P. Gingras and P. A. McClarty, Quantum spin ice: a search for gapless quantum spin liquids in pyrochlore magnets, *Rep. Prog. Phys.* **77**, 056501 (2014).
- [13] S. H. Skjærvø, C. H. Marrows, R. L. Stamps, and L. J. Heyderman, Advances in artificial spin ice, *Nat. Rev. Phys.* **2**, 13 (2020).
- [14] P. Schiffer and C. Nisoli, Artificial spin ice: Paths forward, *Appl. Phys. Lett.* **118**, 110501 (2021).
- [15] C. Nisoli, Topological order of the Rys F-model and its breakdown in realistic square spin ice: Topological sectors of Faraday loops, *Europhys. Lett.* **132**, 47005 (2020).
- [16] V. Schánilec, O. Brunn, M. Horáček, S. Krátký, P. Meluzín, T. Šikola, B. Canals, and N. Rougemaille, Approaching the topological low-energy physics of the F model in a two-dimensional magnetic lattice, *Phys. Rev. Lett.* **129**, 027202 (2022).
- [17] L. D. C. Jaubert, T. Lin, T. S. Opel, P. C. W. Holdsworth, and M. J. P. Gingras, Spin ice thin film: Surface ordering, emergent square ice, and strain effects, *Phys. Rev. Lett.* **118**, 207206 (2017).

- [18] D. M. Arroo and S. T. Bramwell, Experimental measures of topological sector fluctuations in the F-model, *Phys. Rev. B* **102**, 214427 (2020).
- [19] P. W. Anderson, Ordering and antiferromagnetism in ferrites, *Phys. Rev.* **102**, 1008 (1956).
- [20] T. Fennell, M. J. Harris, S. Calder, M. Ruminy, M. Boehm, P. Steffens, M.-H. Lemée-Cailleau, O. Zaharko, A. Cervellino, and S. T. Bramwell, Multiple Coulomb phase in the fluoride pyrochlore CsNiCrF₆, *Nat. Phys.* **15**, 60 (2019).
- [21] Y. Alexanian, E. Lhotel, R. Ballou, C. V. Colin, H. Klein, A. L. Priol, F. Museur, J. Robert, E. Pachoud, P. Lejay, A. Hadj-Azzem, B. Fåk, Q. Berrod, J.-M. Zanotti, E. Suard, C. Dejoie, S. de Brion, and V. Simonet, Collective magnetic state induced by charge disorder in the non-Kramers rare-earth pyrochlore Tb₂ScNbO₇, *Phys. Rev. Mater.* **7**, 094403 (2023).
- [22] K. W. Plumb, H. J. Changlani, A. Scheie, S. Zhang, J. W. Krizan, J. A. Rodriguez-Rivera, Y. Qiu, B. Winn, R. J. Cava, and C. L. Broholm, Continuum of quantum fluctuations in a three-dimensional $S = 1$ Heisenberg magnet, *Nat. Phys.* **15**, 54 (2019).
- [23] L. D. C. Jaubert, M. Haque, and R. Moessner, Analysis of a fully packed loop model arising in a magnetic Coulomb phase, *Phys. Rev. Lett.* **107**, 177202 (2011).
- [24] S. T. Banks and S. T. Bramwell, Magnetic frustration in the context of pseudo-dipolar ionic disorder, *Europhys. Lett.* **97**, 27005 (2012).
- [25] Y. Miyatake, M. Yamamoto, J. J. Kim, M. Toyonaga, and O. Nagai, On the implementation of the ‘heat bath’ algorithms for Monte Carlo simulations of classical Heisenberg spin systems, *J. Phys. C: Solid State Phys.* **19**, 2539 (1986).
- [26] R. Moessner and J. T. Chalker, Low-temperature properties of classical geometrically frustrated antiferromagnets, *Phys. Rev. B* **58**, 12049 (1998).
- [27] M. E. Fisher, Magnetism in one dimensional systems—the Heisenberg model for infinite spin, *Am. J. Phys.* **32**, 343 (1964).
- [28] G. S. Joyce, Classical Heisenberg model, *Phys. Rev.* **155**, 478 (1967).
- [29] N. Shannon, K. Penc and Y. Motome, Nematic, vector-multipole, and plateau-liquid states in the classical $O(3)$ pyrochlore antiferromagnet with biquadratic interactions in applied magnetic field, *Phys. Rev. B* **81**, 184409 (2010).
- [30] K. Binder, H. P. Deutsch, J. D. Reger, M. Scheucher, D. P. Landau, Monte Carlo methods for first-order phase transitions: some recent progress, *Int. J. Mod. Phys. C* **03**, 1025 (1992).
- [31] J. Villain, R. Bidaux, J.-P. Carton, and R. Conte, Order as an effect of disorder, *J. Phys. (Paris)* **41**, 1263 (1980).
- [32] C. L. Henley, Ordering by disorder: Ground state selection in fcc vector antiferromagnets, *J. Appl. Phys.* **61**, 3962 (1987).
- [33] C. L. Henley, Ordering due to disorder in a frustrated vector antiferromagnet, *Phys. Rev. Lett.* **62**, 2056 (1989).
- [34] A. R. McGurn and D. J. Scalapino, One-dimensional ferromagnetic classical-spin-field model, *Phys. Rev. B* **11**, 2552 (1975).
- [35] T. S. Pickles, T. E. Saunders, and J. T. Chalker, Critical phenomena in a highly constrained classical spin system: Néel ordering from the Coulomb phase, *Europhys. Lett.* **84**, 36002 (2008).
- [36] G.-W. Chern, R. Moessner, and O. Tchernyshyov, Partial order from disorder in a classical pyrochlore antiferromagnet, *Phys. Rev. B* **78**, 144418 (2008).
- [37] P. H. Conlon and J. T. Chalker, Absent pinch points and emergent clusters: Further neighbor interactions in the pyrochlore Heisenberg antiferromagnet, *Phys. Rev. B* **81**, 224413 (2010).
- [38] U. Hizi and C. L. Henley, Anharmonic ground state selection in the pyrochlore antiferromagnet, *Phys. Rev. B* **80**, 014407 (2009).
- [39] A. M. Samarakoon, S. A. Grigera, D. A. Tennant, A. Kirste, B. Klemke, P. Strehlow, M. Meißner, J. N. Hallén, L. D. C. Jaubert, C. Castelnuovo, and R. Moessner, Anomalous magnetic noise in an imperfectly flat landscape in the topological magnet Dy₂Ti₂O₇, *Proc. Natl. Acad. Sci. USA* **119**, e2117453119 (2022).
- [40] J. N. Hallén, C. Castelnuovo, and R. Moessner, Thermodynamics and fractal dynamics of nematic spin ice, a doubly frustrated pyrochlore Ising magnet, *Phys. Rev. B* **109**, 014438 (2024).
- [41] N. D. Mermin and H. Wagner, Absence of ferromagnetism or anti-ferromagnetism in one- or two-dimensional isotropic Heisenberg models, *Phys. Rev. Lett.* **17**, 1133 (1966).
- [42] T. E. Saunders and J. T. Chalker, Spin freezing in geometrically frustrated antiferromagnets with weak disorder, *Phys. Rev. Lett.* **98**, 157201 (2007).
- [43] D. A. Keen and A. L. Goodwin, The crystallography of correlated disorder, *Nature (London)* **521**, 303 (2015).
- [44] E. G. Meekel, E. M. Schmidt, L. J. Cameron, A. D. Dharma, H. J. Windsor, S. G. Duyker, A. Minelli, T. Pope, G. Orazio Lepore, B. Slater, C. J. Kepert, and A. L. Goodwin, Truchet-tile structure of a topologically aperiodic metal-organic framework, *Science* **379**, 357 (2023).
- [45] R. Moessner and S. L. Sondhi, Ising models of quantum frustration, *Phys. Rev. B* **63**, 224401 (2001).
- [46] S. Calder, S. R. Giblin, D. R. Parker, P. P. Deen, C. Ritter, J. R. Stewart, S. Rols, and T. Fennell, Neutron scattering and μ SR investigations of the low temperature state of LuCuGaO₄, *J. Phys.: Condens. Matter* **25**, 356002 (2013).
- [47] A. Weinrib and B. I. Halperin, Critical phenomena in systems with long-range-correlated quenched disorder, *Phys. Rev. B* **27**, 413 (1983).
- [48] G. P. Müller, P. F. Bessarab, S. M. Vlasov, F. Lux, N. S. Kiselev, S. Blügel, V. M. Uzdin, and H. Jónsson, Duplication, collapse, and escape of magnetic skyrmions revealed using a systematic saddle point search method, *Phys. Rev. Lett.* **121**, 197202 (2018).